
Higher-Order Spatial Information for Self-Supervised Place Cell Learning

Jared Deighton

Department of Mathematics
The University of Tennessee, Knoxville
Knoxville, TN 37996
jdeight@vols.utk.edu

Wyatt Mackey

Department of Mathematics / NIMBioS
The University of Tennessee, Knoxville
Knoxville, TN 37996
wmackey2@utk.edu

Ioannis Schizas

DEVCOM ARL
Army Research Lab
Aberdeen Proving Ground, MD 21005
ioannis.d.schizas.civ@army.mil

David L. Boothe Jr.

DEVCOM ARL
Army Research Lab
Aberdeen Proving Ground, MD 21005
david.l.boothe7.civ@army.mil

Vasileios Maroulas

Department of Mathematics
The University of Tennessee, Knoxville
Knoxville, TN 37996
vmaroula@utk.edu

Abstract

Mammals navigate novel environments and exhibit resilience to sparse environmental sensory cues via place and grid cells, which encode position in space. While the efficiency of grid cell coding has been extensively studied, the computational role of place cells is less well understood. This gap arises partially because spatial information measures have, until now, been limited to single place cells. We derive and implement a higher-order spatial information measure, allowing for the study of the emergence of multiple place cells in a self-supervised manner. We show that emergent place cells have many desirable features, including high-accuracy spatial decoding. This is the first work in which higher-order spatial information measures that depend solely on place cells' firing rates have been derived and which focuses on the emergence of multiple place cells via self-supervised learning. By quantifying the spatial information of multiple place cells, we enhance our understanding of place cell formation and capabilities in recurrent neural networks, thereby improving the potential navigation capabilities of artificial systems in novel environments without objective location information.

1 Introduction

O'Keefe and Dostrovsky [34] (1971) discovered spatially selective neurons in the hippocampus, which they termed place cells. Place cells form a sparse representation of space by firing at one or several seemingly random locations in small and large environments [40] (Fig. 1 (a)). In 2005, Hafting et al. [22] discovered another set of spatially selective

neurons in the medial entorhinal cortex (MEC), termed grid cells. In contrast to place cells, grid cells exhibit regular hexagonal spatial firing fields. Together, the MEC and hippocampus can encode relative spatial location, without reference to external cues, by integrating linear and angular self-motion [29]. This process is described as path integration or dead reckoning (Fig. 1 (b)).

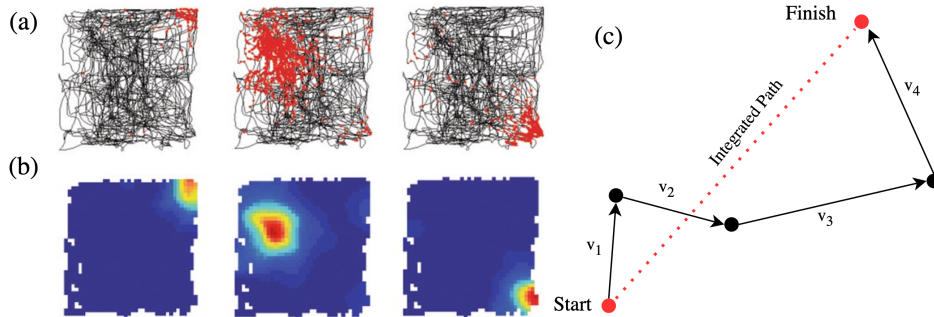


Figure 1: (a) Place cells recorded in hippocampal subarea CA3. Firing locations are shown as red dots on the path of a rat (black). (b) Activity maps of the cells. Red is high firing rate, and blue is no firing. (c) Diagram of the process of path integration. The agent integrates four velocities to determine its current location via the integrated path (red). (a-b) adapted from [50].

In recent years, there has been significant interest in building computational models that mimic mammalian spatial representation [3, 5, 8, 9, 16, 21, 29–31, 43, 47], as a proxy for understanding the utility of underlying neural dynamics. Many implementations train recurrent neural networks (RNNs) for path integration via supervised learning. These models are trained to predict position or to match their output to that of predetermined place cells [9, 46, 47]. Self-supervised learning, which does not rely on external targets, has just recently been applied to the brain’s spatial representations and is not well explored in either the machine learning or neuroscience literature [43]. Previous studies (both supervised and self-supervised) focus on the emergence of grid-cell-like representations, rather than place cells themselves. Theoretical and computational studies on optimal place field location and emergence of place cells have been conducted but are limited to a *single* place cell [45, 52].

In this paper, we make three contributions. First, we define the **joint spatial information rate** of two place cells. Second, we apply this novel measure to investigate RNNs’ capabilities to learn multiple place cells in a self-supervised fashion. By leveraging self-supervised learning, we allow for more flexible representations to arise by only considering the neuronal firing rates in the spatial domain. This allows us to hypothesize about the true nature of place cell emergence and function. Third, we show that learned place cells exhibit strong decoding capabilities, outperforming neurons trained with traditional Skaggs’ spatial information rate [45]. This paper’s result is the first self-supervised learning model focused on the emergence of multiple place cells and their capabilities.

1.1 Related studies

Recurrent neural networks (RNNs) are a promising tool for modeling a network of neurons [3, 5, 9, 8, 20, 29, 43, 46, 47, 51]. By training RNNs to perform path integration based on velocity inputs, grid cell-like representations may form in the hidden layer [3, 9, 43, 46]. This suggests that grid cells, border cells, and other cells observed in MEC, are a natural solution for representing space efficiently given the predominant recurrent connections in the neural circuits [9]. However, it has been recently suggested that the emergence of grid cells in RNNs with velocity inputs may be strongly driven by particular, non-fundamental, and post-hoc implementation choices as opposed to fundamental truths about neural circuits or the loss function(s) they optimize [42]. That is to say, grid cells are not necessarily a natural solution for efficient space representation.

In contrast to grid cells, place cells have received little attention from the computational neuroscience and machine learning communities. Studies in mice and rats have shown that place cells use several factors when determining where to fire in space, including self-motion and the presence of boundaries [7, 27, 33]. In 2017, Keinath et al. [25] showed that the hippocampal map realigns after disorientation, preserving place cell anti-correlated firing, even after realignment within the environment. This suggests that when seeking to understand how place cells encode space, analyzing a pair or group of place cells rather than each one individually is more useful, as they collectively act to form a cognitive map [35, 39]. Information theory [44] has emerged as a technique to determine how much information neurons carry about stimuli [10, 39, 45]. In particular, Quian Quiroga and Panzeri [39] showed that the capacity of a set of neurons to decode position relates to the amount of spatial information conveyed by the neurons. Paramount in the relationship between information theory and neuroscience is the formulation of the spatial information rate by Skaggs et al. [45], which has seen tremendous use in characterizing how well single neurons encode space in both experimental studies [1, 2, 12–15, 18, 23, 32, 36] and in theoretical studies [48, 52].

2 Spatial information rates

Here, we create a framework to analyze the spatial information rate of two place cells. Eventually, our higher-order measure will be used in a criterion for an RNN to perform path integration. First, we recall Skaggs’ spatial information rate of one neuron.

2.1 Single neuron

Skaggs et al. [45] define the spatial information rate (in bits/s) of a single place cell A , across discrete space $X = \{x_1 \dots x_{n_x}\}$, as

$$I_{sec}(A : X) = \sum_{j=1}^{n_x} \lambda_A(x_j) \log_2 \left(\frac{\lambda_A(x_j)}{\bar{\lambda}_A} \right) p(x_j), \quad (1)$$

where, x_j for $j = 1, \dots, n_x$ is the spatial vector, $p(x_j)$ is the probability of the agent being at location x_j , $\lambda_A(x_j)$ is the mean firing rate of the place cell A at location x_j , and $\bar{\lambda}_A = \sum_{j=1}^{n_x} \lambda_A(x_j) p(x_j)$ is the mean firing rate of place cell A over the entire spatial domain.

Measuring the information quantity in bits/spike is often more useful to distinguish place cell information content. This is denoted as I_{spike} and defined by

$$I_{spike}(A : X) = \frac{1}{\bar{\lambda}_A} I_{sec}(A : X) = \sum_{j=1}^{n_x} \frac{\lambda_A(x_j)}{\bar{\lambda}_A} \log_2 \left(\frac{\lambda_A(x_j)}{\bar{\lambda}_A} \right) p(x_j), \quad (2)$$

As initially described by Skaggs, I_{spike} measures the *specificity* of the cell [45]. When the spatial domain is consistent, for shorthand, we write $I_{spike}(A : X) = I_{spike}(A)$.

2.2 Multiple neurons

In this section, we derive a higher-order spatial information rate for two neurons, called the joint spatial information rate. This crucial step allows for the analysis of multiple place cells via information theory.

Definition 2.1. Consider two place cells A and B , and let $r \in [-1, 1]$ be the Pearson’s correlation coefficient between place cells over some spatial domain X . If p is a probability mass function over a discrete spatial domain X , then the **joint spatial information rate** (in

bits/s) of place cells A and B is

$$\begin{aligned}
I_{sec}(A, B) = \sum_{x \in X} & \left[p(x) r \sqrt{\lambda_{a,b}(x)} \log_2 \left(\frac{\sqrt{\lambda_{a,b}(x)}}{\tilde{\lambda}_{a,b}} \right) \right. \\
& + p(x) \left(\lambda_a(x) - r \sqrt{\lambda_{a,b}(x)} \right) \log_2 \left(\frac{\lambda_a(x) - r \sqrt{\lambda_{a,b}(x)}}{\bar{\lambda}_a - r \tilde{\lambda}_{a,b}} \right) \\
& \left. + p(x) \left(\lambda_b(x) - r \sqrt{\lambda_{a,b}(x)} \right) \log_2 \left(\frac{\lambda_b(x) - r \sqrt{\lambda_{a,b}(x)}}{\bar{\lambda}_b - r \tilde{\lambda}_{a,b}} \right) \right], \tag{3}
\end{aligned}$$

where $\lambda_a(x)\lambda_b(x) = \lambda_{a,b}(x)$ and $\sum_{x \in X} p(x) \sqrt{\lambda_{a,b}(x)} = \tilde{\lambda}_{a,b}$.

Spatial information may be generated via any combinations of neurons A and B spiking or not spiking. In Construction D.1, we derive the information rate for each of the four scenarios, which together form Equation (3). We can likewise define $I_{spike}(A, B)$ by choosing an appropriate normalization term:

$$I_{spike}(A, B) = \frac{1}{\Lambda_{A,B}} I_{sec}(A, B), \tag{4}$$

where $\Lambda_{A,B} = \sum_{x \in X} p(x) \frac{\lambda_a(x) + \lambda_b(x)}{2} = \frac{\bar{\lambda}_a + \bar{\lambda}_b}{2}$. As desired, $I_{spike}(A, B)$ is in units of bits/spike. Furthermore, as shown in Theorem D.3, $I_{spike}(A, B) = I_{spike}(B, A)$, and $I_{spike}(A, A) = I_{spike}(A)$.

Our definition of $I_{spike}(A, B)$ has two main limitations. First, it is not well-defined for all possible collections of firing rates $\{\lambda_A(x_i)\}_{i=1}^{n_x}$, $\{\lambda_B(x_i)\}_{i=1}^{n_x}$. We circumvent this by assigning the value 0 to terms not well-defined (as is commonly done for $0 \log(0)$ in information-theoretic quantities). Furthermore, we have yet to construct a proof that $I_{spike}(A, B)$ is non-negative when only considering well-defined terms. However, our experiments have not encountered a negative joint spatial information rate.

Definition 2.2. For n_p place cells P_1, P_2, \dots, P_{n_p} , we construct the **spatial information matrix**, $J \in \mathbb{R}^{n_p \times n_p}$ whose entries are given by

$$J_{i,j} = I_{spike}(P_i, P_j). \tag{5}$$

Here, J contains the joint spatial information rates (in bits/spike) between all pairs of neurons in the spatial domain. As a result of Theorem D.3, J is symmetric, and its diagonal consists of the Skaggs' spatial information rates of the individual place cells, $I_{spike}(P_i)$ for $i = 1, \dots, n_p$. If $\lambda_1, \dots, \lambda_{n_p}$ are the eigenvalues of J such that $|\lambda_1| \geq |\lambda_2| \geq \dots \geq |\lambda_{n_p}|$, we have that $\lambda_i \in \mathbb{R}$ for all $i = 1, \dots, n_p$. Furthermore, if $J_{i,j} = I_{spike}(P_i, P_j) \geq 0$ for all i, j (as is the case for our experiments), then, $\lambda_1 \geq 0$ by the Perron-Frobenius Theorem [17].

3 Methods

3.1 RNN architecture and training

We implement an RNN for self-supervised learning of place cells via information theory. Initial activations $P_0 \in \mathbb{R}^{n_p}$ are encoded by $E \in \mathbb{R}^{n_p \times n_s}$, and each subsequent hidden state $G_i \in \mathbb{R}^{n_s}$ evolves from $G_{i-1} \in \mathbb{R}^{n_s}$ with a velocity input $v_i \in \mathbb{R}^2$ for $i = 1, \dots, n_x$ (Fig. 2). We obtain place cell activations $P_i = W G_i \in \mathbb{R}^{n_p}$ via decoder $W \in \mathbb{R}^{n_s \times n_p}$. The collection of place cell activations forms $P \in \mathbb{R}^{n_x \times n_p}$, where $P_{x,j}$ represents the firing rate of place cell j at spatial index x .

We use the spatial information matrix J (Definition 2.2), associated with place cell activations P to analyze global place cell information and calculate epoch loss (Fig. 2). To learn place cells via J , one could choose to optimize all the entries of J or its leading eigenvalue,

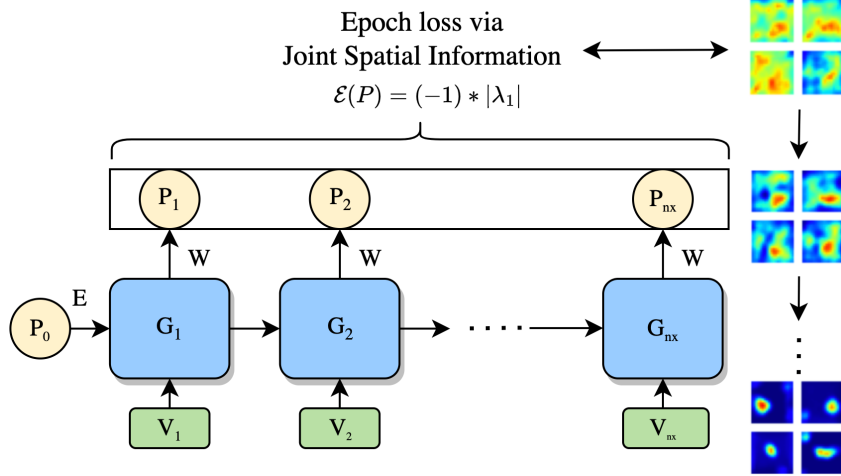


Figure 2: A diagram of RNN architecture used to perform self-supervised learning. As training progresses (right), the neuron’s firing fields become more place cell-like.

λ_1 . These values are highly correlated (Remark D.4), and optimizing along either choice leads to similar results (Fig. 9). For our experiments, we choose to focus on the optimization of λ_1 . That is, to increase information efficiency, we minimize

$$\mathcal{E}_{higher-order}(P) = (-1) * |\lambda_1|, \quad (6)$$

where λ_1 is the leading eigenvalue of J . Calculating I_{spike} from place cell activations P requires a probability mass function across the trajectories n_x steps. For simplicity, we assume this to be a discrete uniform distribution for all trajectories in the spatial domain, that is $p(x_i) = \frac{1}{n_x}$ for all $i \in \{1, \dots, n_x\}$. Additional experimental details, including hyperparameters, are listed in Appendix A.

As a baseline, we compare the results of maximizing higher-order information (Equation (6)) with the results of maximizing single-order information according to Skaggs’ spatial information rate [45]. This latter loss function is given by,

$$\mathcal{E}_{skaggs}(P) = (-1) * \sum_{i=1}^{n_p} I_{spike}(P[:, i]), \quad (7)$$

where $P[:, i] \in \mathbb{R}^{n_x}$ is the i th column of P .

3.2 Place cell score

To compare place cells produced by optimizing along our higher-order information measure with control experiments, we construct a **place cell score**. Our place cell score is an approximately equal combination of three characterizing features of place cells: (i) smoothness of the firing rate; (ii) binary activation of the place field; and (iii) sparsity of the place field. Each of these factors is a key feature of the place fields of *in vitro* place cells [6, 28]. The place cell score PC of a place cell P is then given by

$$PC_{score}(P, \epsilon) = 100 * Smoothness(P) + 10 * Binary(P, \epsilon) - 10 * Sparsity(P), \quad (8)$$

where ϵ is a small number and a hyperparameter of the system. To compute the smoothness, binary activity, and sparsity scores of a place cell, we measure the firing rates of the place cell P across the entire arena and normalize values between 0 and 1. Then, if $\Pi \in \mathbb{R}^{h \times h}$ is the binned matrix of activations across a square arena from place cell P at a

spatial resolution h , we use the following metrics:

$$\text{Smoothness}(P) = \frac{1}{h^2} \sum_{i=1}^h \sum_{j=1}^h |\Pi_{i,j} - \tilde{\Pi}_{i,j}|, \quad (9)$$

$$\text{Binary}(P, \epsilon) = P(\Pi < \epsilon) + P(\Pi > 1 - \epsilon), \quad (10)$$

$$\text{Sparsity}(P) = \frac{(\sum_{i=1}^h \sum_{j=1}^h \Pi_{i,j})^2}{\sum_{i=1}^h \sum_{j=1}^h \Pi_{i,j}^2}, \quad (11)$$

where $\tilde{\Pi} \in \mathbb{R}^{h \times h}$ is the smoothed matrix of activations from place cell P . For our purposes, $\tilde{\Pi}$ is acquired via Gaussian Blur with kernel size (5,5) and kernel standard deviations $\sigma_x = \sigma_y = 1$. We may also calculate the spatial information rate of the learned place cells across the entire arena via

$$I_{\text{spike}}(P) = \sum_{i=1}^h \sum_{j=1}^h \frac{\Pi_{i,j}}{\bar{\Pi}} \log_2 \left(\frac{\Pi_{i,j}}{\bar{\Pi}} \right) p(\text{bin}_{i,j}), \quad (12)$$

where $\bar{\Pi} = \sum_{i=1}^h \sum_{j=1}^h p(\text{bin}_{i,j}) \Pi_{i,j}$. For simplicity, we assume the agent is equally likely to be in any spatial bin, i.e. $p(\text{bin}_{i,j}) = 1/h^2$ for all i, j .

4 Results

RNNs trained to optimize higher-order spatial information learn place cell-like receptive responses and path-invariant representations. Our training method outperforms classical Skaggs' information maximization as place cells consider other neurons' activity. Place cells learned through higher-order spatial optimization exhibit superior spatial decoding properties and uniformity compared to place cells learned by optimizing the Skaggs' spatial information rate. These improvements are accompanied by greater place cell scores in the higher-order place cells.

4.1 Place cells arise via self-supervised learning

Training with higher-order spatial information significantly improves spatial encoding by enhancing the quantity and quality of place cells. In Fig. 3, we compare place cell scores of place cells learned via higher-order spatial information to those learned via Skaggs' spatial information.

Training with higher-order spatial information results in a greater median place cell score (0.971) than neurons trained with Skaggs loss (-0.656), while both improve upon untrained neurons (-13.28) (Fig. 3 (b)). In Appendix C, we show that higher-order spatial information consistently outperforms Skaggs spatial information in learning place-cell-like representations regardless of changes in training parameters (batch size, number of hidden units, etc.). These improvements underscore the effectiveness of including higher-order spatial information when optimizing neural representations of space. Place cell activation maps from all models are available in the supplementary materials.

4.2 Neural decoding

We consider two experiments to ensure the decoding abilities of the learned place cells. In each experiment, we attempt to decode the agent's location from binarized place cell activations. By turning the activations into binary values, spatial decoding must be done by relating a combination of active neurons to an area in the arena. Consequently, each decoding algorithm operates with the sole knowledge of which neurons are in an "active" state. Each experiment is repeated ten times, i.e. once for each model, for a given number of place cells to obtain an average score. We display the results in Fig. 4.

The first decoding task (Fig. 4 (a)) is to decode the position in the arena using leave-one-out classification. In leave-one-out classification, one data point is reserved for testing and

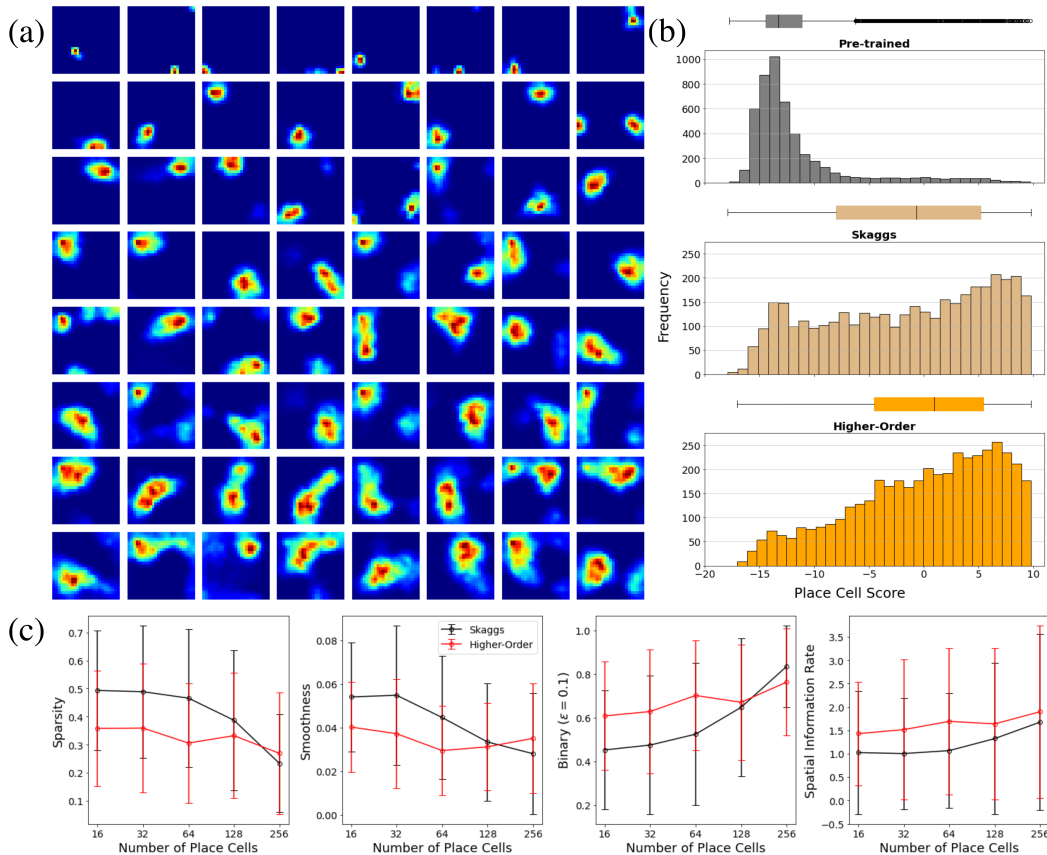


Figure 3: (a) Activation maps of top 64 learned place cells from a model trained with higher-order spatial information, normalized to be between 0 and 1, and sorted by place cell score (Equation (8)). Fig. 8 shows all 128 place cell activation maps from this model. (b) Original and trained place cell score box plots and histograms. Place cell scores are recorded across 50 total models for each loss function with varying place cell sizes. (c) Mean (\pm standard deviation) sparsity, smoothness, binarity ($\epsilon = 0.1$), and spatial information rate (Equations (9- 12)) of trained place cells as the number of place cells increases.

the remaining data points are used to train a Naive Bayes' Classifier (see [48] for details). This procedure is repeated multiple times so that each firing rate value is used once for testing. In Fig. 4, we apply this using data from 10 trajectories (1000 positions) for each model. Neurons trained with higher-order spatial information can predict the position with high precision, mirroring the simulated trajectory in all areas of the arena (Fig. 4 (a)). Furthermore, these neurons consistently outperform neurons trained with Skaggs' spatial information rate (Fig. 4 (b)).

To generate Fig. 4 (c - d), we train a support vector machine (SVM) with a linear kernel to predict which quadrant of the region the agent is in from the binarized neural input. Higher-order spatial information outperforms Skaggs spatial information by nearly 10% when training just 16 neurons, and performs comparably for greater than 16 neurons.

These experiments demonstrate that the place cells learned via self-supervised learning with higher-order spatial information encode space better than neurons trained with Skaggs' spatial information. Combined with the results from Section 4.1, we conclude that self-supervised learning with higher-order spatial information allows for precise spatial decoding with more place cell-like neural representations than previously attainable via Skaggs' spatial information.

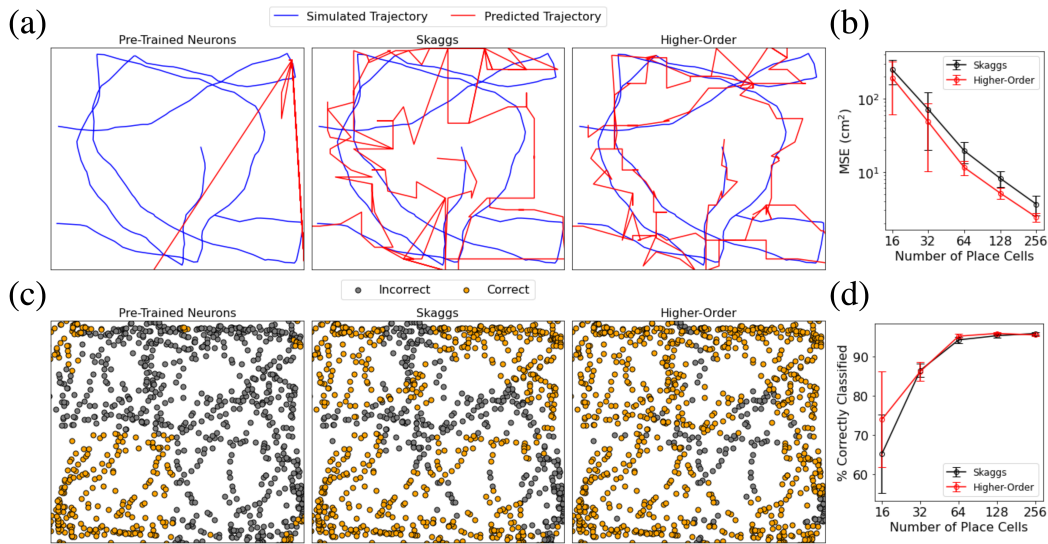


Figure 4: Comparison of decoding capabilities of binarized neurons before and after training. (a) Simulated and predicted trajectories leave-one-out classification with 128 neurons. (b) Skaggs vs higher-order leave-one-out decoding mean square error (MSE) as the number of trained place cells increases. The mean (\pm standard deviation) of MSE across experiments is shown. (c) Correctly (orange) and incorrectly (grey) classified activations from a support vector machine (SVM) for quadrant classification using 16 neurons. (d) Skaggs vs higher-order quadrant classification accuracy. The mean (\pm standard deviation) of accuracy across experiments is shown.

4.3 Path invariance and uniformity

A key feature of any collection of neurons encoding spatial representation is its path invariance [43]. That is, two trajectories that begin and end at the same position should have identical final neural representations (Fig. 5 (a)). Furthermore, the firing fields of place cells are known to create a sparse representation of space, with consistent activity responses in the absence of additional stimuli [41], a property we refer to as uniformity.

To test for path invariance of our place cell representations, we form two trajectories by randomly shuffling a sequence of velocity vectors. We then compare the place cell activity by measuring the Euclidean distance of the discrepancy (Equation (13)) between the two trajectories: if $P_{n_x}, P_{\text{shuffled } n_x} \in \mathbb{R}^{Np}$ are re-scaled activations at the final position, then the path invariance discrepancy D is

$$D = \|P_{n_x} - P_{\text{shuffled } n_x}\|_2^2. \quad (13)$$

We measure D for 1000 pairs of trajectories for each model, and display results in Fig. 5 (b).

Our models trained with joint spatial information demonstrate exceptional performance (Fig. 5 (b)), achieving an average (\pm standard deviation) path invariance discrepancy of 0.004 ± 0.024 for Skaggs' optimization and 0.022 ± 0.066 for higher-order optimization, while pre-trained models had a path invariance discrepancy of 1.024 ± 0.859 . This further indicates that self-supervised learning combined with spatial information optimization results in models that successfully encode space.

To measure the uniformity of spatial representations, we calculate the standard deviation in the number of highly active place cells at each discretized spatial region. A lower standard deviation suggests that the place cells have become more uniform as their firing fields disperse evenly across the domain. Place cells learn anti-correlated firing only by training with higher-order spatial information (Equation (6)), as shown in Fig. 6 (a). Training with the Skaggs loss function optimizes each cell's spatial information rate (Equation (7)) and is agnostic toward the firing of the other cells. In Fig. 6 (b), we show that place cells trained

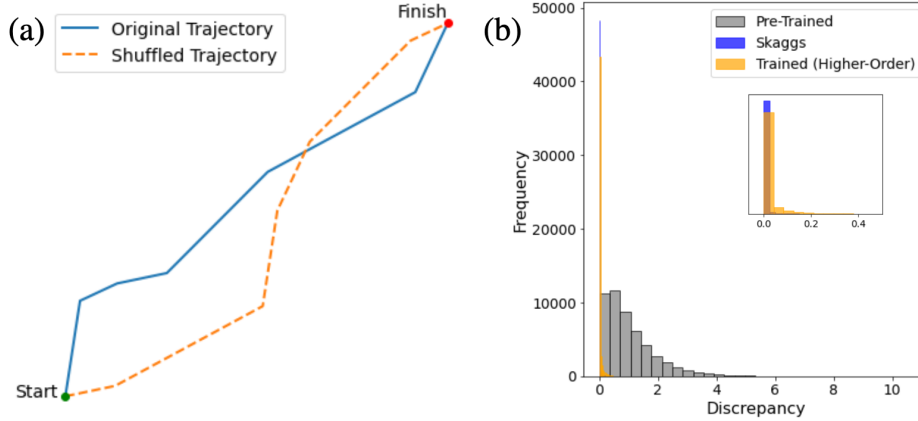


Figure 5: (a) Two trajectories formed by shuffling the order of velocities. Since both trajectories end at the same location, neural representations at the final position should be identical despite different paths to get there. (b) Histogram of path invariance discrepancy across 1000 trajectories from all pre-trained models, models trained with Skaggs’ spatial information, and models trained with higher-order spatial information.

with higher-order spatial information result in greater uniformity than those trained with Skaggs’ spatial information.

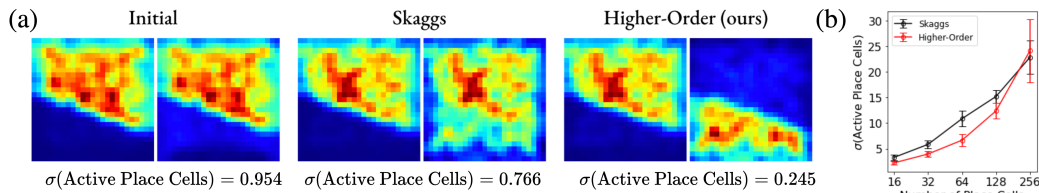


Figure 6: (a) Comparison of two place cell firing fields in which the initial cells fire in the same region. Standard deviation in active place cells decreases as firing fields separate. (b) Mean (\pm standard deviation) of the standard deviation in the number of place cells with high activity (defined as exceeding 20% of the peak firing rate of the rate map) as the number of trained place cells varies.

5 Discussion

To create an internal map of the world, the brain uses a multitude of specialized neurons to encode spatial information. Here, we formulate the first rigorous definition of joint spatial information (Definition 2.1). This crucial step allows us to effectively quantify the efficiency of a population of neurons in conveying spatial information. We demonstrate that this novel criterion allows RNNs to learn place cell-like representations with superior position decoding performance. Like true place cells, the learned place cells are path invariant and exhibit uniform spatial representations in the absence of external stimuli.

It has been suggested that for place cell-based recurrent architectures to learn grid cell-like hidden layer representations, the readout code must be translation invariant [3, 46]. This property is not likely present in *in vivo* place cells, which over-represent certain locations, and is not present in those learned by our models [11, 19]. As a result, the units in the hidden layer of our models bore little resemblance to that of grid cells. This phenomenon has been observed in supervised models with realistic place cell-like heterogeneous responses [42]. In total, a model that simultaneously produces grid and place cells in an unsupervised fashion is still at large.

A natural extension of our work is to construct spatial information measures for $n \geq 3$ place cells without the use of eigenvalue analysis. However, such measures may be less computationally efficient than our proposed method for large n , as they would likely scale exponentially with the number of place cells (as opposed to our method, which scales quadratically). This will require further mathematical analysis, possibly diverging from the techniques used thus far.

Our results lend themselves nicely to the investigation of place cell remapping. Studies have shown that place cells form statistically independent representations of pairs of environments [1]. Our model can achieve different representations in geometrically identical environments by altering the initialization of its parameters, including the probability of the agent visiting various domain regions. Future work will be focused on merging information-theoretic methods with models of episodic memory believed to exist in the hippocampus [4, 49].

Overall, our work displays the success of unifying advanced information theory with neuroscience and its applications to machine learning. The result is a widely applicable formula for place cell efficiency, which lays the foundation for more questions regarding place cell formation, function, and role in the mammalian brain.

Acknowledgments and Disclosure of Funding

This work has been partially supported by the Army Research Laboratory Cooperative Agreement No W911NF2120186.

References

- [1] Charlotte B Alme, Chenglin Miao, Karel Jezek, Alessandro Treves, Edvard I Moser, and May-Britt Moser. Place cells in the hippocampus: eleven maps for eleven rooms. *Proceedings of the National Academy of Sciences*, 111(52):18428–18435, 2014.
- [2] Dmitriy Aronov, Rhino Nevers, and David W Tank. Mapping of a non-spatial dimension by the hippocampal–entorhinal circuit. *Nature*, 543(7647):719–722, 2017.
- [3] Andrea Banino, Caswell Barry, Benigno Uria, Charles Blundell, Timothy Lillicrap, Piotr Mirowski, Alexander Pritzel, Martin J Chadwick, Thomas Degris, Joseph Modayil, et al. Vector-based navigation using grid-like representations in artificial agents. *Nature*, 557(7705):429–433, 2018.
- [4] Marcus K Benna and Stefano Fusi. Place cells may simply be memory cells: Memory compression leads to spatial tuning and history dependence. *Proceedings of the National Academy of Sciences*, 118(51):e2018422118, 2021.
- [5] Yoram Burak and Ila R Fiete. Accurate path integration in continuous attractor network models of grid cells. *PLoS computational biology*, 5(2):e1000291, 2009.
- [6] Jan Bures, Andre A Fenton, Yu Kaminsky, and L Zinyuk. Place cells and place navigation. *Proceedings of the National Academy of Sciences*, 94(1):343–350, 1997.
- [7] Guifen Chen, John A King, Neil Burgess, and John O’Keefe. How vision and movement combine in the hippocampal place code. *Proceedings of the National Academy of Sciences*, 110(1):378–383, 2013.
- [8] Jonathan J Couey, Aree Witoelar, Sheng-Jia Zhang, Kang Zheng, Jing Ye, Benjamin Dunn, Rafal Czapkowski, May-Britt Moser, Edvard I Moser, Yasser Roudi, et al. Recurrent inhibitory circuitry as a mechanism for grid formation. *Nature neuroscience*, 16(3):318–324, 2013.
- [9] Christopher J Cueva and Xue-Xin Wei. Emergence of grid-like representations by training recurrent neural networks to perform spatial localization. *arXiv preprint arXiv:1803.07770*, 2018.
- [10] Peter Dayan and Laurence F Abbott. *Theoretical neuroscience: computational and mathematical modeling of neural systems*. MIT press, 2005.
- [11] David Dupret, Joseph O’neill, Barty Pleydell-Bouverie, and Jozsef Csicsvari. The reorganization and reactivation of hippocampal maps predict spatial memory performance. *Nature neuroscience*, 13(8):995–1002, 2010.
- [12] André A Fenton, Hsin-Yi Kao, Samuel A Neymotin, Andrey Olypher, Yevgeniy Vayntrub, William W Lytton, and Nandor Ludvig. Unmasking the ca1 ensemble place code by exposures to small and large environments: more place cells and multiple, irregularly arranged, and expanded place fields in the larger space. *Journal of Neuroscience*, 28(44):11250–11262, 2008.
- [13] Arseny Finkelstein, Dori Derdikman, Alon Rubin, Jakob N Foerster, Liora Las, and Nachum Ulanovsky. Three-dimensional head-direction coding in the bat brain. *Nature*, 517(7533):159–164, 2015.
- [14] Loren M Frank, Emery N Brown, and Matthew Wilson. Trajectory encoding in the hippocampus and entorhinal cortex. *Neuron*, 27(1):169–178, 2000.
- [15] Hongjun Fu, Gustavo A Rodriguez, Mathieu Herman, Sheina Emrani, Eden Nahmani, Geoffrey Barrett, Helen Y Figueroa, Eliana Goldberg, S Abid Hussaini, and Karen E Duff. Tau pathology induces excitatory neuron loss, grid cell dysfunction, and spatial memory deficits reminiscent of early alzheimer’s disease. *Neuron*, 93(3):533–541, 2017.
- [16] Mark C Fuhs and David S Touretzky. A spin glass model of path integration in rat medial entorhinal cortex. *Journal of Neuroscience*, 26(16):4266–4276, 2006.

- [17] Feliks Ruvimovich Gantmakher. *The theory of matrices*, volume 131. American Mathematical Soc., 2000.
- [18] Richard J Gardner, Erik Hermansen, Marius Pachitariu, Yoram Burak, Nils A Baas, Benjamin A Dunn, May-Britt Moser, and Edvard I Moser. Toroidal topology of population activity in grid cells. *Nature*, 602(7895):123–128, 2022.
- [19] Jeffrey L Gauthier and David W Tank. A dedicated population for reward coding in the hippocampus. *Neuron*, 99(1):179–193, 2018.
- [20] Alex Graves and Alex Graves. Long short-term memory. *Supervised sequence labelling with recurrent neural networks*, pages 37–45, 2012.
- [21] Alexis Guanella, Daniel Kiper, and Paul Verschure. A model of grid cells based on a twisted torus topology. *International journal of neural systems*, 17(04):231–240, 2007.
- [22] Torkel Hafting, Marianne Fyhn, Sturla Molden, May-Britt Moser, and Edvard I Moser. Microstructure of a spatial map in the entorhinal cortex. *Nature*, 436(7052):801–806, 2005.
- [23] Robin Hayman, Madeleine A Verriotis, Aleksandar Jovalekic, André A Fenton, and Kathryn J Jeffery. Anisotropic encoding of three-dimensional space by place cells and grid cells. *Nature neuroscience*, 14(9):1182–1188, 2011.
- [24] R.A. Horn and C.R. Johnson. *Matrix Analysis*. Cambridge University Press, 1990. ISBN 9780521386326. URL <https://books.google.com/books?id=PLYQN0ypTwEC>.
- [25] Alex T Keinath, Joshua B Julian, Russell A Epstein, and Isabel A Muzzio. Environmental geometry aligns the hippocampal map during spatial reorientation. *Current Biology*, 27(3):309–317, 2017.
- [26] Diederik P Kingma and Jimmy Ba. Adam: A method for stochastic optimization. *arXiv preprint arXiv:1412.6980*, 2014.
- [27] Colin Lever, Tom Wills, Francesca Cacucci, Neil Burgess, and John O’Keefe. Long-term plasticity in hippocampal place-cell representation of environmental geometry. *Nature*, 416(6876):90–94, 2002.
- [28] Etan J Markus, Carol A Barnes, Bruce L McNaughton, Victoria L Gladden, and William E Skaggs. Spatial information content and reliability of hippocampal ca1 neurons: effects of visual input. *Hippocampus*, 4(4):410–421, 1994.
- [29] Bruce L McNaughton, Francesco P Battaglia, Ole Jensen, Edvard I Moser, and May-Britt Moser. Path integration and the neural basis of the ‘cognitive map’. *Nature Reviews Neuroscience*, 7(8):663–678, 2006.
- [30] Edward C Mitchell, Brittany Story, David Boothe, Piotr J Franaszczuk, and Vasileios Maroulas. A topological deep learning framework for neural spike decoding. *Biophysical Journal*, 2024.
- [31] Farzana Nasrin, Christopher Oballe, David Boothe, and Vasileios Maroulas. Bayesian topological learning for brain state classification. In *2019 18th IEEE International Conference On Machine Learning And Applications (ICMLA)*, pages 1247–1252. IEEE, 2019.
- [32] Edward H Nieh, Manuel Schottdorf, Nicolas W Freeman, Ryan J Low, Sam Lewallen, Sue Ann Koay, Lucas Pinto, Jeffrey L Gauthier, Carlos D Brody, and David W Tank. Geometry of abstract learned knowledge in the hippocampus. *Nature*, 595(7865):80–84, 2021.
- [33] John O’Keefe. Place units in the hippocampus of the freely moving rat. *Experimental neurology*, 51(1):78–109, 1976.
- [34] John O’Keefe and Jonathan Dostrovsky. The hippocampus as a spatial map: preliminary evidence from unit activity in the freely-moving rat. *Brain research*, 1971.

- [35] John O’keefe and Lynn Nadel. *The hippocampus as a cognitive map*. Oxford university press, 1978.
- [36] Jake Ormond and John O’Keefe. Hippocampal place cells have goal-oriented vector fields during navigation. *Nature*, 607(7920):741–746, 2022.
- [37] Adam Paszke, Sam Gross, Francisco Massa, Adam Lerer, James Bradbury, Gregory Chanan, Trevor Killeen, Zeming Lin, Natalia Gimelshein, Luca Antiga, et al. Pytorch: An imperative style, high-performance deep learning library. *Advances in neural information processing systems*, 32, 2019.
- [38] F. Pedregosa, G. Varoquaux, A. Gramfort, V. Michel, B. Thirion, O. Grisel, M. Blondel, P. Prettenhofer, R. Weiss, V. Dubourg, J. Vanderplas, A. Passos, D. Cournapeau, M. Brucher, M. Perrot, and E. Duchesnay. Scikit-learn: Machine learning in Python. *Journal of Machine Learning Research*, 12:2825–2830, 2011.
- [39] Rodrigo Quian Quiroga and Stefano Panzeri. Extracting information from neuronal populations: information theory and decoding approaches. *Nature Reviews Neuroscience*, 10(3):173–185, 2009.
- [40] P Dylan Rich, Hua-Peng Liaw, and Albert K Lee. Large environments reveal the statistical structure governing hippocampal representations. *Science*, 345(6198):814–817, 2014.
- [41] Etienne Save, Arnaud Cressant, Catherine Thinus-Blanc, and Bruno Poucet. Spatial firing of hippocampal place cells in blind rats. *Journal of Neuroscience*, 18(5):1818–1826, 1998.
- [42] Rylan Schaeffer, Mikail Khona, and Ila Fiete. No free lunch from deep learning in neuroscience: A case study through models of the entorhinal-hippocampal circuit. *Advances in Neural Information Processing Systems*, 35:16052–16067, 2022.
- [43] Rylan Schaeffer, Mikail Khona, Tzuhsuan Ma, Cristobal Eyzaguirre, Sanmi Koyejo, and Ila Fiete. Self-supervised learning of representations for space generates multi-modular grid cells. *Advances in Neural Information Processing Systems*, 36, 2024.
- [44] Claude Elwood Shannon. A mathematical theory of communication. *The Bell system technical journal*, 27(3):379–423, 1948.
- [45] William Skaggs, Bruce McNaughton, and Katalin Gothard. An information-theoretic approach to deciphering the hippocampal code. *Advances in neural information processing systems*, 5, 1992.
- [46] Ben Sorscher, Gabriel Mel, Surya Ganguli, and Samuel Ocko. A unified theory for the origin of grid cells through the lens of pattern formation. *Advances in neural information processing systems*, 32, 2019.
- [47] Ben Sorscher, Gabriel C Mel, Samuel A Ocko, Lisa M Giocomo, and Surya Ganguli. A unified theory for the computational and mechanistic origins of grid cells. *Neuron*, 111(1):121–137, 2023.
- [48] Bryan C Souza, Rodrigo Pavão, Hindiael Belchior, and Adriano BL Tort. On information metrics for spatial coding. *Neuroscience*, 375:62–73, 2018.
- [49] Larry R Squire, Craig EL Stark, and Robert E Clark. The medial temporal lobe. *Annu. Rev. Neurosci.*, 27:279–306, 2004.
- [50] Tor Stensola and Edvard I Moser. Grid cells and spatial maps in entorhinal cortex and hippocampus. *Micro-, meso-and macro-dynamics of the brain*, pages 59–80, 2016.
- [51] David Sussillo, Mark M Churchland, Matthew T Kaufman, and Krishna V Shenoy. A neural network that finds a naturalistic solution for the production of muscle activity. *Nature neuroscience*, 18(7):1025–1033, 2015.
- [52] Yihong Wang, Xuying Xu, and Rubin Wang. The place cell activity is information-efficient constrained by energy. *Neural Networks*, 116:110–118, 2019.

A Experimental details

Our code was implemented in PyTorch [37] and is available at (removed for anonymization, see supplementary materials). Our methodology closely aligns with the frameworks established in the publicly available codes used in [46, 47] and in [9]. Hyperparameters for our experiments are listed in Table 1. The majority of the code was run using a 2.8 GHz Quad-Core Intel Core i7 processor with 16 GB of memory. Here, training a single higher-order spatial information model with 16 place cells and 256 hidden units for 100 epochs takes roughly 16 seconds. Training 64 place cells and 1028 hidden units for 30 epochs takes roughly 2 minutes. Code to train models with 256 place cells and to perform sensitivity analysis C was run using a Tesla K80 GPU with 64GB of memory.

Table 1: Hyperparameters used for training the networks.

Hyperparameter	Value
Batch size	40
Sequence length	100
Learning rate	1e-4
Number of place cells	16, 32, 64, 128, 256
Number of hidden units	256, 1028, 1028, 1028, 2048
Periodic boundary conditions	False
Arena Size (m)	0.5
RNN nonlinearity	$ReLU(\cdot)$
Optimizer	Adam [26]
Weight decay	None

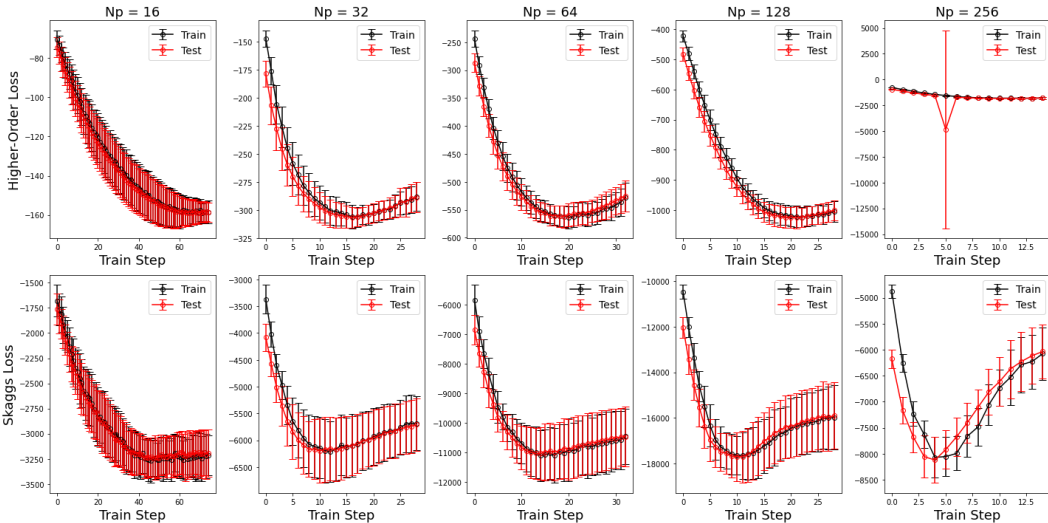


Figure 7: Mean (\pm standard deviation) train and test loss from 10 experiments for each N_p (number of place cells) and loss function.

Trajectory generation: We generate trajectories in a two-dimensional square arena using previously published codes found in [46, 47]. In short, the agent’s initial position is randomly drawn from a uniform distribution across the set of possible positions. Then, a sequence of random speeds and turns is constructed to create the trajectory. Trajectories can be freely generated. We reserve 40 unique trajectories for testing and train the model on 40 unique trajectories for each epoch. Training and testing summaries are in Fig. 7.

Leave-One-out classification. Leave-one-out classification for spatial decoding was performed using Scikit-learn’s [38] Naive Bayes classifier and KBinsDiscretizer. For each trained model, we pass 10 trajectories (1000 positions) through the network to obtain place cell activations. The 1000 positions are binned using the KBinsDiscretizer with 100 bins

in each dimension. Then, all but one of the firing rate-location pairs are used to estimate posterior probabilities (i.e. to fit the classifier). Then, the Naive Bayes classifier predicts the position of the left-out firing rate. This process is repeated so that every firing rate value is used for testing. The predicted positions (given as a predicted bin) are then transformed back to a predicted position in \mathbb{R}^2 using `KBinsDiscretizer`'s inverse transform, from which the mean-squared error with the true positions is calculated.

Support Vector Machine. Support Vector Machine: Quadrant classification for spatial decoding was performed using Scikit-learn's [38] support vector machine (SVM) and `KBinsDiscretizer`. First, we generate many trajectories (1000) to obtain place cell activations at various positions for each model. Now, to create the quadrant classes the positions are binned using the `KBinsDiscretizer` with 2 bins in each dimension. We use 10000 firing rate-quadrant pairs to fit an SVM with a linear kernel. Then, the SVM is tested on 1000 separate samples to obtain the quadrant classification accuracy.

B Additional place cell maps

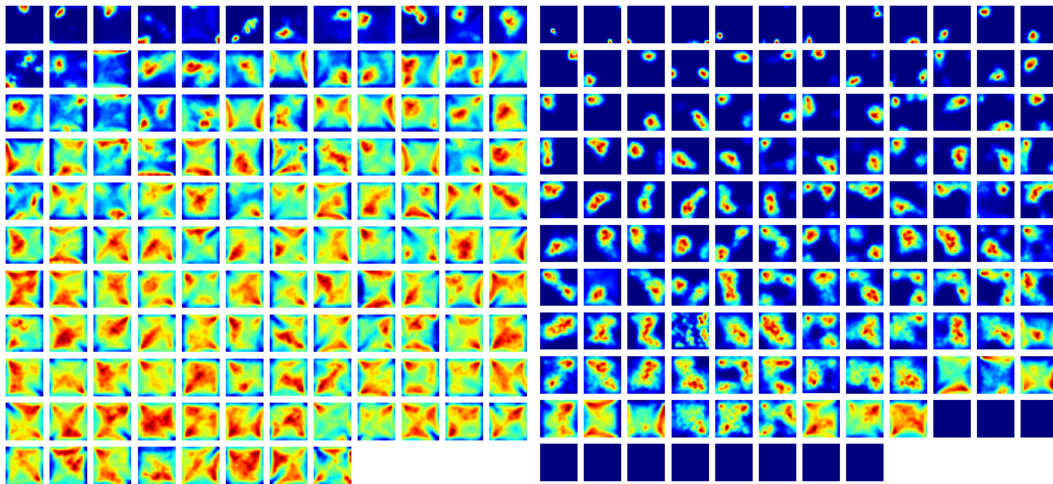


Figure 8: Pre-trained and trained (with higher-order spatial information) place cell activations for 128 place cells. Each place cell's activations are normalized between 0 and 1. The top 64 are displayed in Fig. 3.

Additional activation maps for all models referred to in Section 4 are available in the supplementary materials.

C Sensitivity

To test the effect of training with higher-order spatial information as compared to Skaggs spatial information rate across training parameters, we train three distinct models (each with 32 place cells) for all possible combinations of the following parameters:

- Arena Size (in meters): 0.25, 0.75, 1, 1.5
- Number of Hidden Units (N_g): 256, 512, 1028
- Learning Rate: 0.001, 0.0001, 0.00001
- Batch Size: 10, 40, 80
- Sequence Length: 40, 80, 120

We implement a simple stopping criterion during training, in which training halts if the current epoch loss is greater than the mean of the previous three epoch losses (provided

the model has trained for at least five epochs). The mean place cell score (\pm standard deviation) is presented below across various pairs of parameters.

Skaggs PC Score ($N_p = 32$)

Arena Size (m)	0.25	0.75	1	1.5
Ng				
256	-2.81 \pm 6.01	-4.22 \pm 6.04	-3.24 \pm 5.98	-1.52 \pm 4.61
512	-1.93 \pm 5.45	-3.65 \pm 5.36	-2.6 \pm 5.52	-0.48 \pm 3.99
1028	-1.67 \pm 5.22	-2.98 \pm 5.15	-2.11 \pm 5.5	0.42 \pm 3.64

Learning Rate	1e-03	1e-04	1e-05
Ng			
256	-6.62 \pm 5.49	-0.16 \pm 5.45	-2.07 \pm 6.03
512	-4.48 \pm 5.26	-1.43 \pm 4.92	-0.58 \pm 5.06
1028	-1.93 \pm 4.96	-1.65 \pm 4.93	-1.17 \pm 4.75

Batch Size	10	40	80
Ng			
256	-6.3 \pm 6.66	-4.54 \pm 6.01	1.99 \pm 4.31
512	-6.09 \pm 6.32	-3.75 \pm 5.59	3.34 \pm 3.34
1028	-5.68 \pm 6.38	-3.16 \pm 5.47	4.08 \pm 2.79

Sequence Length	40	80	120
Ng			
256	-1.87 \pm 5.28	-2.76 \pm 5.68	-4.22 \pm 6.02
512	-1.25 \pm 4.87	-2.1 \pm 4.95	-3.15 \pm 5.42
1028	-1.03 \pm 4.81	-1.52 \pm 4.84	-2.21 \pm 4.99

Learning Rate	1e-03	1e-04	1e-05
Arena Size (m)			
0.25	-3.57 \pm 4.67	1.24 \pm 3.66	0.75 \pm 3.92
0.75	-4.03 \pm 5.39	-0.94 \pm 5.77	-1.44 \pm 5.52
1	-4.36 \pm 5.41	-1.78 \pm 5.76	-1.81 \pm 5.83
1.5	-5.42 \pm 5.48	-2.83 \pm 5.22	-2.6 \pm 5.85

Batch Size	10	40	80
Arena Size (m)			
0.25	-3.54 \pm 4.73	-2.0 \pm 4.58	3.96 \pm 2.94
0.75	-5.73 \pm 6.82	-3.32 \pm 6.09	2.62 \pm 3.77
1	-6.32 \pm 7.09	-4.32 \pm 6.16	2.7 \pm 3.76
1.5	-8.5 \pm 7.16	-5.63 \pm 5.93	3.28 \pm 3.46

Sequence Length	40	80	120
Arena Size (m)			
0.25	-0.3 \pm 4.05	-0.35 \pm 3.89	-0.93 \pm 4.31
0.75	-1.21 \pm 5.34	-2.04 \pm 5.44	-3.16 \pm 5.9
1	-1.41 \pm 5.19	-2.9 \pm 5.7	-3.63 \pm 6.11
1.5	-2.61 \pm 5.36	-3.21 \pm 5.61	-5.03 \pm 5.58

Batch Size	10	40	80
Learning Rate			
1e-03	-5.2 \pm 6.95	-2.81 \pm 5.8	4.77 \pm 2.55
1e-04	-5.07 \pm 6.71	-2.56 \pm 5.66	3.81 \pm 3.47
1e-05	-7.79 \pm 5.69	-6.08 \pm 5.61	0.84 \pm 4.42

Sequence Length	40	80	120
Learning Rate			
1e-03	-0.76 \pm 5.25	-0.82 \pm 4.9	-1.66 \pm 5.15
1e-04	-0.77 \pm 4.98	-1.18 \pm 5.29	-1.88 \pm 5.57
1e-05	-2.62 \pm 4.72	-4.38 \pm 5.29	-6.03 \pm 5.7

Sequence Length	40	80	120
Batch Size			
10	4.31 \pm 2.83	3.45 \pm 3.43	1.65 \pm 4.18
40	-3.09 \pm 5.55	-3.9 \pm 5.78	-4.46 \pm 5.74
80	-5.38 \pm 6.58	-5.92 \pm 6.27	-6.77 \pm 6.51

Higher-Order PC Score ($N_p = 32$)

Arena Size (m)	0.25	0.75	1	1.5
Ng				
256	-1.6 \pm 5.54	-2.9 \pm 6.25	-2.21 \pm 5.93	-0.61 \pm 4.47
512	-0.46 \pm 5.48	-2.27 \pm 5.96	-1.22 \pm 5.91	0.2 \pm 4.1
1028	-0.33 \pm 5.52	-2.35 \pm 5.3	-1.28 \pm 5.76	0.68 \pm 3.96

Learning Rate	1e-03	1e-04	1e-05
Ng			
256	-6.79 \pm 5.3	2.16 \pm 5.75	-0.86 \pm 5.59
512	-4.78 \pm 5.17	1.03 \pm 5.96	0.93 \pm 4.96
1028	-2.25 \pm 4.76	-1.28 \pm 5.46	1.09 \pm 5.18

Batch Size	10	40	80
Ng			
256	-4.76 \pm 6.37	-3.16 \pm 6.08	2.43 \pm 4.19
512	-4.1 \pm 6.67	-2.42 \pm 5.95	3.71 \pm 3.47
1028	-4.48 \pm 6.55	-2.16 \pm 5.8	4.2 \pm 3.05

Sequence Length	40	80	120
Ng			
256	-0.82 \pm 5.26	-1.94 \pm 5.65	-2.73 \pm 5.73
512	-0.22 \pm 5.13	-0.88 \pm 5.31	-1.7 \pm 5.65
1028	-0.43 \pm 5.0	-0.82 \pm 5.14	-1.2 \pm 5.27

Learning Rate	1e-03	1e-04	1e-05
Arena Size (m)			
0.25	-3.68 \pm 4.57	2.12 \pm 4.16	1.83 \pm 3.8
0.75	-4.3 \pm 5.18	1.42 \pm 6.1	0.49 \pm 5.26
1	-4.73 \pm 5.29	0.13 \pm 6.45	-0.1 \pm 5.87
1.5	-5.72 \pm 5.27	-1.13 \pm 6.18	-0.66 \pm 6.06

Batch Size	10	40	80
Arena Size (m)			
0.25	-2.66 \pm 4.79	-1.49 \pm 4.81	4.43 \pm 2.93
0.75	-3.7 \pm 6.65	-1.67 \pm 6.12	2.97 \pm 3.77
1	-4.69 \pm 7.29	-2.68 \pm 6.33	2.67 \pm 3.99
1.5	-6.74 \pm 7.4	-4.49 \pm 6.52	3.72 \pm 3.58

Sequence Length	40	80	120
Arena Size (m)			
0.25	0.1 \pm 4.24	0.36 \pm 4.03	-0.18 \pm 4.26
0.75	-0.09 \pm 5.14	-0.99 \pm 5.65	-1.32 \pm 5.75
1	-0.34 \pm 5.5	-1.85 \pm 5.95	-2.51 \pm 6.16
1.5	-1.63 \pm 5.65	-2.38 \pm 5.82	-3.5 \pm 6.04

Batch Size	10	40	80
Learning Rate			
1e-03	-2.43 \pm 7.63	-0.68 \pm 6.56	5.02 \pm 2.97
1e-04	-2.73 \pm 6.64	-0.76 \pm 5.8	4.65 \pm 3.29
1e-05	-8.18 \pm 5.33	-6.31 \pm 5.46	0.67 \pm 4.44

Sequence Length	40	80	120
Learning Rate			
1e-03	0.86 \pm 5.75	0.74 \pm 5.54	0.3 \pm 5.88
1e-04	0.58 \pm 5.14	0.31 \pm 5.38	0.28 \pm 5.21
1e-05	-2.92 \pm 4.5	-4.69 \pm 5.17	-6.21 \pm 5.56

Sequence Length	40	80	120
Batch Size			
10	4.47 \pm 2.9	3.56 \pm 3.6	2.31 \pm 4.21
40	-1.97 \pm 5.85	-2.86 \pm 5.98	-2.92 \pm 6.0
80	-3.98 \pm 6.65	-4.35 \pm 6.51	-5.02 \pm 6.44

D Higher-Order Spatial Information

Construction D.1 (Derivation of the Joint Spatial Information Rate). Here, we construct the joint spatial information rate of two place cells A and B . For some discrete space X , let $\lambda_a(x)$ and $\lambda_b(x)$ be the firing rate of place cells A and B at location $x \in X$, respectively. Let A_x and B_x denote the events where A and B spike at position x during Δt and A_x^c and B_x^c denote the complements.

Now, we estimate the correlation between two place cells r as the Pearson's correlation over the entire spatial domain and create the joint distribution of the cells firing during a small time Δt by treating each distribution of a place cell firing during Δt as a Bernoulli distribution. Then, $R = \text{COV}(A, B) = r\sqrt{\lambda_a(x)\Delta t(1-\lambda_a(x)\Delta t)\lambda_b(x)\Delta t(1-\lambda_b(x)\Delta t)}$ where r is the correlation coefficient between place cells A and B , and we have

$$\begin{aligned} P(A_x \cap B_x) &= R + \lambda_a(x)\lambda_b(x)(\Delta t)^2 \\ P(A_x \cap B_x^c) &= \lambda_a(x)\Delta t(1 - \lambda_b(x)\Delta t) - R \\ P(A_x^c \cap B_x) &= (1 - \lambda_a(x)\Delta t)\lambda_b(x)\Delta t - R \\ P(A_x^c \cap B_x^c) &= (1 - \lambda_a(x)\Delta t)(1 - \lambda_b(x)\Delta t) + R \end{aligned}$$

Neglecting terms higher than Δt , we have $R \approx r\sqrt{\lambda_a(x)\lambda_b(x)}\Delta t$ and

$$\begin{aligned} P(A_x \cap B_x) &= r\sqrt{\lambda_a(x)\lambda_b(x)}\Delta t \\ P(A_x \cap B_x^c) &= \lambda_a(x)\Delta t - r\sqrt{\lambda_a(x)\lambda_b(x)}\Delta t \\ P(A_x^c \cap B_x) &= \lambda_b(x)\Delta t - r\sqrt{\lambda_a(x)\lambda_b(x)}\Delta t \\ P(A_x^c \cap B_x^c) &= 1 - \lambda_a(x)\Delta t - \lambda_b(x)\Delta t + r\sqrt{\lambda_a(x)\lambda_b(x)}\Delta t \end{aligned}$$

We also have, regardless of location $E[(P(A_x \cap B_x))] = \sum_x p(x)r\sqrt{\lambda_a(x)\lambda_b(x)}\Delta t$ and similarly for the other scenarios.

Then, the mutual information between the joint distribution and space is

$$I(A, B) = \sum_x \sum_{\omega_x \in \Omega_x} p(x)P(\omega_x) \log_2 \left(\frac{P(\omega_x)}{E[P(\omega_x)]} \right) \quad (14)$$

where $\Omega_x = \{A_x \cap B_x, \dots, A_x^c \cap B_x^c\}$ is the set of possible outcomes at location x . In Lemma D.2, we show that the final term ($\omega_x = A_x^c \cap B_x^c$) goes to zero when dropping terms higher than Δt . Thus, expanding Equation (14) and a short simplification yields,

$$\begin{aligned} I(A, B) &= \Delta t \sum_x p(x)r\sqrt{\lambda_a(x)\lambda_b(x)} \log_2 \left(\frac{\sqrt{\lambda_a(x)\lambda_b(x)}}{\sum_x p(x)\sqrt{\lambda_a(x)\lambda_b(x)}} \right) \\ &\quad + p(x)[\lambda_a(x) - r\sqrt{\lambda_a(x)\lambda_b(x)}] \log_2 \left(\frac{\lambda_a(x) - r\sqrt{\lambda_a(x)\lambda_b(x)}}{\sum_x p(x)[\lambda_a(x) - r\sqrt{\lambda_a(x)\lambda_b(x)}]} \right) \\ &\quad + p(x)[\lambda_b(x) - r\sqrt{\lambda_a(x)\lambda_b(x)}] \log_2 \left(\frac{\lambda_b(x) - r\sqrt{\lambda_a(x)\lambda_b(x)}}{\sum_x p(x)[\lambda_b(x) - r\sqrt{\lambda_a(x)\lambda_b(x)}]} \right) \end{aligned}$$

Then, using the series expansion of $I(A, B)$ around t , we have that the first time derivative is approximated by

$$\begin{aligned} I(A, B)' &\approx \sum_x p(x) r \sqrt{\lambda_a(x) \lambda_b(x)} \log_2 \left(\frac{\sqrt{\lambda_a(x) \lambda_b(x)}}{\sum_x p(x) \sqrt{\lambda_a(x) \lambda_b(x)}} \right) \\ &\quad + p(x) [\lambda_a(x) - r \sqrt{\lambda_a(x) \lambda_b(x)}] \log_2 \left(\frac{\lambda_a(x) - r \sqrt{\lambda_a(x) \lambda_b(x)}}{\sum_x p(x) [\lambda_a(x) - r \sqrt{\lambda_a(x) \lambda_b(x)}]} \right) \\ &\quad + p(x) [\lambda_b(x) - r \sqrt{\lambda_a(x) \lambda_b(x)}] \log_2 \left(\frac{\lambda_b(x) - r \sqrt{\lambda_a(x) \lambda_b(x)}}{\sum_x p(x) [\lambda_b(x) - r \sqrt{\lambda_a(x) \lambda_b(x)}]} \right) \end{aligned}$$

This is the definition of $I_{sec}(A, B)$ the joint spatial information rate. We may write more succinctly,

$$\begin{aligned} I_{sec}(A, B) &= \sum_x p(x) r \sqrt{\lambda_{a,b}(x)} \log_2 \left(\frac{\sqrt{\lambda_{a,b}(x)}}{\bar{\lambda}_{a,b}} \right) \\ &\quad + p(x) \left(\lambda_a(x) - r \sqrt{\lambda_{a,b}(x)} \right) \log_2 \left(\frac{\lambda_a(x) - r \sqrt{\lambda_{a,b}(x)}}{\bar{\lambda}_a - r \bar{\lambda}_{a,b}} \right) \\ &\quad + p(x) \left(\lambda_b(x) - r \sqrt{\lambda_{a,b}(x)} \right) \log_2 \left(\frac{\lambda_b(x) - r \sqrt{\lambda_{a,b}(x)}}{\bar{\lambda}_b - r \bar{\lambda}_{a,b}} \right) \end{aligned}$$

where $\sum_x p(x) \lambda_a(x) = \bar{\lambda}_a$, $\sum_x p(x) \lambda_b(x) = \bar{\lambda}_b$, $\sum_x p(x) \sqrt{\lambda_{a,b}(x)} = \bar{\lambda}_{a,b}$, and $\lambda_a(x) \lambda_b(x) = \lambda_{a,b}(x)$.

Finally as is done for I_{sec} , we may write the joint information of two PCs in units of bits/spike by defining,

$$I_{spike}(A, B) = \frac{1}{\Lambda_{A,B}} I_{sec}(A, B)$$

where $\Lambda_{A,B} = \sum_x p(x) \frac{\lambda_a(x) + \lambda_b(x)}{2} = \frac{\bar{\lambda}_a + \bar{\lambda}_b}{2}$. This is chosen so that $I_{spike}(A, A) = I_{spike}(A)$.

Lemma D.2 (No-firing term provides no information). Here we show that the no-firing term from Equation (14) goes to zero.

Proof. First, notice

$$\begin{aligned} &\log_2 \left(\frac{1 - \Delta t (\lambda_a(x) + \lambda_b(x) - r \sqrt{\lambda_a(x) \lambda_b(x)})}{\sum_x p(x) [1 - \Delta t (\lambda_a(x) + \lambda_b(x) - r \sqrt{\lambda_a(x) \lambda_b(x)})]} \right) \\ &= \log_2 \left(1 - \Delta t (\lambda_a(x) + \lambda_b(x) - r \sqrt{\lambda_a(x) \lambda_b(x)}) \right) - \log_2 \left(\sum_x p(x) - \Delta t \sum_x p(x) [\lambda_a(x) + \lambda_b(x) - r \sqrt{\lambda_a(x) \lambda_b(x)}] \right) \\ &= \log_2 \left(1 - \Delta t (\lambda_a(x) + \lambda_b(x) - r \sqrt{\lambda_a(x) \lambda_b(x)}) \right) - \log_2 \left(1 - \Delta t \sum_x p(x) [\lambda_a(x) + \lambda_b(x) - r \sqrt{\lambda_a(x) \lambda_b(x)}] \right) \end{aligned}$$

Using the Taylor series $\log_2(1 - x\Delta t) \approx -\frac{x\Delta t}{\ln(2)}$ we can approximate these terms by

$$\begin{aligned} &\log_2 \left(\frac{1 - \Delta t (\lambda_a(x) + \lambda_b(x) - r \sqrt{\lambda_a(x) \lambda_b(x)})}{\sum_x p(x) [1 - \Delta t (\lambda_a(x) + \lambda_b(x) - r \sqrt{\lambda_a(x) \lambda_b(x)})]} \right) \\ &\approx -\Delta t \frac{\lambda_a(x) + \lambda_b(x) - r \sqrt{\lambda_a(x) \lambda_b(x)}}{\ln(2)} + \Delta t \frac{\sum_x p(x) [\lambda_a(x) + \lambda_b(x) - r \sqrt{\lambda_a(x) \lambda_b(x)}]}{\ln(2)} \end{aligned}$$

Thus, focusing on the last term of $I(A, B)$ in Equation (14),

$$\begin{aligned} & \sum_x p(x) [1 - \Delta t (\lambda_a(x) + \lambda_b(x) - r \sqrt{\lambda_a(x) \lambda_b(x)})] \log_2 \left(\frac{1 - \Delta t (\lambda_a(x) + \lambda_b(x) - r \sqrt{\lambda_a(x) \lambda_b(x)})}{\sum_x p(x) [1 - \Delta t (\lambda_a(x) + \lambda_b(x) - r \sqrt{\lambda_a(x) \lambda_b(x)})]} \right) \\ &= \sum_x p(x) \frac{\Delta t}{\ln(2)} \left(\sum_x p(x) [\lambda_a(x) + \lambda_b(x) - r \sqrt{\lambda_a(x) \lambda_b(x)}] - (\lambda_a(x) + \lambda_b(x) - r \sqrt{\lambda_a(x) \lambda_b(x)}) \right) = 0 \end{aligned}$$

□

Theorem D.3 (Spatial Information Properties). We show that the described properties hold. First, $I_{spike}(A, B) = I_{spike}(B, A)$ holds trivially. Next, we show that $I_{spike}(A, A) = I_{spike}(A)$

Proof. Notice that if $A = B$, then we have the following:

$$\begin{aligned} \bar{\lambda}_b &= \bar{\lambda}_a \\ \sqrt{\lambda_{a,b}(x)} &= \sqrt{\lambda_a(x) \lambda_b(x)} = \sqrt{\lambda_a^2(x)} = \lambda_a(x) \\ \bar{\lambda}_{a,b} &= \sum_x p(x) \sqrt{\lambda_{a,b}(x)} = \sum_x p(x) \lambda_a(x) = \bar{\lambda}_a \\ \Lambda_{a,b} &= \frac{\bar{\lambda}_a + \bar{\lambda}_b}{2} = \frac{\bar{\lambda}_a + \bar{\lambda}_a}{2} = \bar{\lambda}_a \\ r &= 1 \end{aligned}$$

Thus,

$$\begin{aligned} I_{spike}(A, A) &= \frac{1}{\bar{\lambda}_a} I_{sec}(A, A) = \frac{1}{\bar{\lambda}_a} \sum_{x \in X} \left[p(x) \lambda_a(x) \log_2 \left(\frac{\lambda_a(x)}{\bar{\lambda}_a} \right) \right. \\ &\quad + p(x) (\lambda_a(x) - \lambda_a(x)) \log_2 \left(\frac{\lambda_a(x) - \lambda_a(x)}{\bar{\lambda}_a - \bar{\lambda}_a} \right) \\ &\quad \left. + p(x) (\lambda_a(x) - \lambda_a(x)) \log_2 \left(\frac{\lambda_a(x) - \lambda_a(x)}{\bar{\lambda}_a - \bar{\lambda}_a} \right) \right] \\ &= \sum_{x \in X} \left[p(x) \frac{\lambda_a}{\bar{\lambda}_a}(x) \log_2 \left(\frac{\lambda_a(x)}{\bar{\lambda}_a} \right) + p(x) 0 \log(0/0) + p(x) 0 \log(0/0) \right] \end{aligned}$$

Lastly, setting terms which are not well-defined to zero,

$$I_{spike}(A, A) = \sum_{x \in X} p(x) \frac{\lambda_a}{\bar{\lambda}_a}(x) \log_2 \left(\frac{\lambda_a(x)}{\bar{\lambda}_a} \right) = I_{spike}(A)$$

□

Remark D.4 (Eigenvalues of Spatial Information Matrix). Suppose we have a data matrix $P \in \mathbb{R}^{n_x \times n_p}$ representing n_p place cell firing rates across a trajectory of length n_x . That is, $P_{i,j} = \lambda_j(x_i)$, place cell j 's mean firing rate at spatial location x_i . From P , we construct $J \in \mathbb{R}^{n_p \times n_p}$ with $J_{i,j} = I_{spike}(P_i, P_j)$, the joint spatial information rate between place cells i, j , and the trajectory. Let, $R(J, v)$ be the the Rayleigh quotient [24] of J with nonzero vector v such that $\|v\|_2 = 1$, and $S(J)$ be the sum of the entries of J . That is,

$$\begin{aligned} R(J, v) &= v^T J v = \sum_{i=1}^{n_p} \sum_{j=1}^{n_p} v_i J_{ij} v_j \\ S(J) &= \sum_{i=1}^{n_p} \sum_{j=1}^{n_p} J_{ij} \end{aligned}$$

It follows that $\max_{v, \|v\|_2=1} R(J, v) = \lambda_1$ where λ_1 is the leading eigenvalue of J . When $v_i > 0$ for all $i = 1, \dots, n_p$, we have that λ_1 is positively correlated with $S(J)$ (Fig. 9).

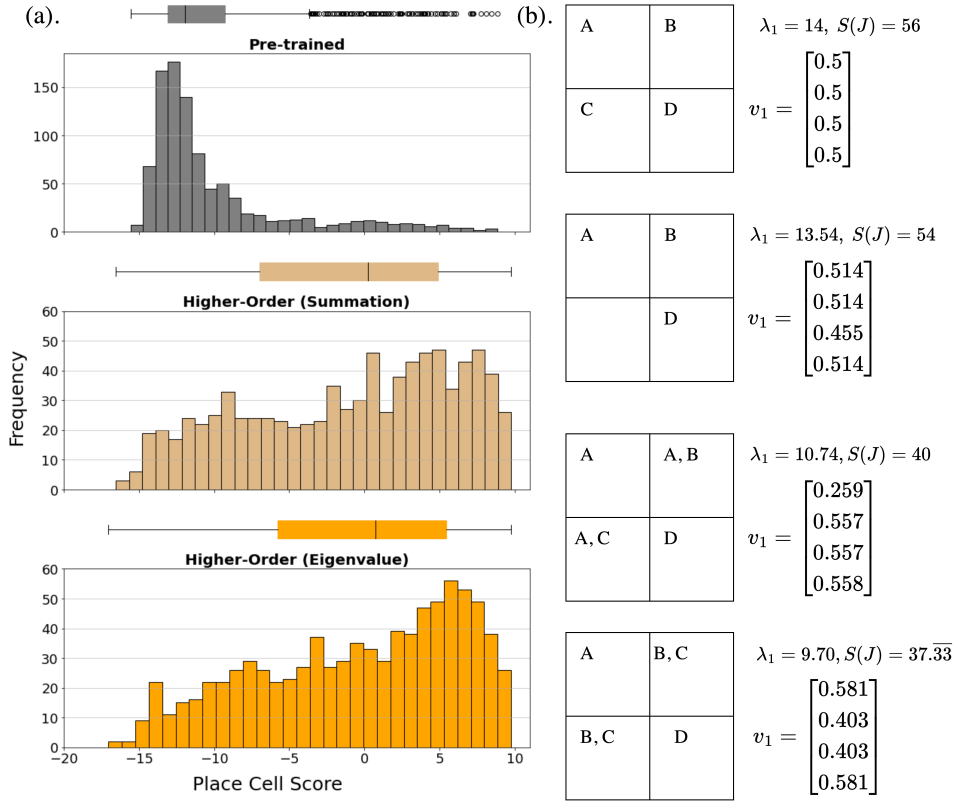


Figure 9: (a) Place cell box plots and histograms across 20 models (10 trained with 32 place cells, 10 with 64). Comparison in place cell score (Equation (8)) is shown between models trained via maximizing $S(J)$, the summation of the entries of J versus maximizing the leading eigenvalue of J . (b) Comparison between the leading eigenvalue of the spatial information matrix J , λ_1 , and $S(J)$ across four scenarios. Consider four neurons, A, B, C, and D in a simple four-quadrant square arena. If the letter of a neuron appears in a quadrant, then we set the firing rate of the neuron in that quadrant to 1 spike/sec. The corresponding leading eigenpair (λ_1, v_1) as well as $S(J)$ are shown for each scenario.